3-27-1997

A Soil-Canopy-Atmosphere Model for Use in Satellite Microwave Remote Sensing

Venkataraman Lakshmi
University of South Carolina - Columbia, vlakshmi@geol.sc.edu

Eric F. Wood

Bhaskar J. Choudhury

Publication Info

Published in *Journal of Geophysical Research*, Volume 102, Issue D6, 1997, pages 6911-6927.
Lakshmi, V., Wood, E. F., & Choudhury, B. J. (1997). A soil-canopy-atmosphere model for use in satellite microwave remote sensing. *Journal of Geophysical Research, 102* (D6), 6911-6927.

JOURNAL OF GEOPHYSICAL RESEARCH, VOL. 102, NO. D6, PAGES 6911–6927, MARCH 27, 1997

A soil-canopy-atmosphere model for use in satellite microwave remote sensing

Venkataraman Lakshmi,[1] Eric F. Wood, and Bhaskar J. Choudhury[2]

Water Resources Program, Department of Civil Engineering and Operations Research, Princeton University, Princeton, New Jersey

Abstract. Regional and global scale studies of land-surface–atmosphere interactions require the use of observations for calibration and validation. In situ field observations are not representative of the distributed nature of land surface characteristics, and large-scale field experiments are expensive undertakings. In light of these requirements and shortcomings, satellite observations serve our purposes adequately. The use of satellite data in land surface modeling requires developing a hydrological model with a thin upper layer to be compatible with the nature of the satellite observations and that would evaluate the soil moisture and soil temperature of a thin layer close to the surface. This paper outlines the formulation of a thin layer hydrological model for use in simulating the soil moistures and soil temperatures. This thin layer hydrological model is the first step in our attempt to use microwave brightness temperature data for regional soil moisture estimation. The hydrological model presented here has been calibrated using five years (1980–1984) of daily streamflow data for the Kings Creek catchment. The calibrated parameters are used to validate the daily streamflows for the next 5 year period (1985–1989). The comparison of surface soil moistures and surface temperatures for the period of the Intensive Field Campaigns (IFCs) during the First ISLSCP (International Satellite Land Surface Climatology Project) Field Experiment (FIFE) in 1987 is carried out and yields good results. The thin layer hydrological model is coupled with a canopy radiative transfer model and an atmospheric attenuation model to create a coupled soil-canopy-atmosphere model in order to study the effect of the vegetation and the soil characteristics on the Special Sensor Microwave Imager (SSM/I) brightness temperatures. The sensitivities of the brightness temperatures to the soil and vegetation is examined in detail. The studies show that increasing leaf area index masks the polarization difference signal originating at the soil surface.

1. Introduction

Surface soil moisture is perhaps the most important indicator of land surface response to atmospheric forcing and provides feedback to the atmosphere. The proper estimation of soil moisture would greatly enhance our understanding of land-surface–atmosphere interactions. Surface soil moisture plays an important role in partitioning rainfall into infiltration and runoff. The land surface evaporation and transpiration depend on the amount of soil moisture available. Together, surface temperature and soil moisture determine the land surface heat and water balance. In large-scale modeling, the soil moisture and temperature are important in deciding the depth of the planetary boundary layer, circulation/wind patterns [*Mahfouf et al.*, 1987; *Lanicci et al.*, 1987; *Zhang et al.*, 1982] and regional water and energy budgets. It is therefore important for improved modeling of these quantities and the use of observational data on scales comparable to the modeling scales. Satellite data are useful in this regard. Research in and utilization of remotely sensed data is important for the purposes of understanding spatial variability and regional scales and in verifying land surface parameterizations [*Wood*, 1991].

Projects like the Global Energy and Water Experiment (GCIP) Continental Scale International Project (GCIP) involve the development and testing of hydrological models on a continental scale over the southern plains of the United States. The availability of data sets for the validation of continental scale soil moisture simulations would be very useful. There are many advantages to remote sensing as a method of soil moisture determination as compared to field sampling. Field sampling is point based and does not give a clear picture of the variation of the soil moisture over an area. Accuracy (difference between the actual soil moisture pattern and the interpolated soil moisture pattern) of interpolation schemes depends on the closeness of the sampled soil moisture data points and the heterogeneity of the soil moisture distribution. In the case where the correlation lengths of soil moisture are smaller than the measurement spatial interval, ground-based data collection may result in the biased sampling of the soil moisture.

Satellite remote sensing offers spatial coverage and a certain temporal frequency in monitoring soil moisture from space. The microwave frequencies of the electromagnetic spectrum are the most sensitive to the variations of soil moisture [*Schmugge*, 1985] due to the polar nature of water. This change in dielectric constant of the soil (caused by changes in soil moisture) is recorded as changes in the radiation emitted by

[1]Now at General Sciences Corporation, Laboratory for Atmospheres, NASA Goddard Space Flight Center, Greenbelt, Maryland.

[2]Now at Hydrological Sciences Branch, NASA Goddard Space Flight Center, Greenbelt, Maryland.

Paper number 96JD03763.
0148-0227/97/96JD-03763$09.00

the soil in the microwave region. Our choice here to use passive microwave remote sensing was dictated by the presence of the Special Sensor Microwave Imager (SSM/I), a microwave sensor with global coverage and daily temporal coverage. In addition, the SSM/I is a very stable, sensitive, and well-calibrated sensor [*Hollinger et al.*, 1990], which makes it a very appealing choice. In addition, the SSM/I is the only remote sensor at this time which can be used for soil moisture sensing.

The motivation for the development and testing of a thin layer model for land hydrology stems from the desire to use satellite remote sensing for purposes of soil moisture estimation. The SSM/I is a four-frequency (19, 22, 37, and 85 GHz), dual polarization (horizontal and vertical except for 22 GHz, which has only horizontal polarization) sensor. The resolution of the SSM/I is about 56 km at 19 GHz and 33 km at 37 GHz, which are the frequencies being used for soil moisture sensing. The surface temperature and soil moisture form the boundary conditions for microwave radiation emanating from the soil. The penetration depth of the SSM/I sensor would be in the order of one tenth of the wavelength to a wavelength [*Ulaby et al.*, 1986], which means the contribution thickness to the microwave radiation would be 0.1 to 1.5 cm in the case of 19 GHz and 0.08 to 0.8 cm in the case of 37 GHz. Therefore the hydrological model should predict the surface temperature and soil moisture for a thin upper layer (1 cm).

Most of the hydrological models have an upper layer which corresponds to the root zone depth [*Famiglietti et al.*, 1994a, b; *Liang et al.*, 1994]. This may be anywhere between 5–10 cm and 50 cm. We are specifically interested in the top 1 cm layer. Also, these models do not validate with regard to both soil moisture and soil temperature. An omission in both of these models is the adequate parameterization of moisture gradient driven flux from the lower layer to the upper layer to replenish the soil moisture of the upper layer. This aspect of soil moisture dynamics is very important when modeling the soil column, especially during the morning (0600) overpass of the SSM/I sensor, prior to which the upper layer has been depleted by evaporation during the previous day and is replenished during the nighttime hours when the soil evaporation is low. A thin layer model of soil hydrology with a 1 cm upper layer based on assumptions validated by comparison with a more detailed finite element approach [*Mahrt et al.*, 1984] to minimize truncation errors is used.

The purpose of this paper is to develop a thin layer hydrological model for water and energy balance that can be used to predict the top 1 cm layer soil moisture and the surface temperature and to understand the processes and the sensitivities of the SSM/I brightness temperatures to vegetation and soil moisture. This is followed by investigations of the effect of heterogeneities in land surface characteristics and rainfall input on simulated brightness temperatures [*Lakshmi et al.*, 1996a] and simulations of regional scale surface soil moistures using the thin layer hydrological model for a period of a year (August 1987 to July 1988) and estimation using SSM/I 19 and 37 GHz brightness temperature data and their comparison [*Lakshmi et al.*, 1996b].

2. Thin layer soil hydrological model

This section describes the thin layer hydrological model. The model is divided into two layers: the top layer is 1 cm thick and the bottom layer is 99 cm thick. The model includes infiltration of rainfall, runoff, bare soil evaporation from the top layer, the exchange fluxes between the top layer and the bottom layer, subsurface drainage from the bottom layer, and transpiration by vegetation from the bottom layer. The water balance for the two soil layers (1.0 cm top layer thickness) and the top canopy interception storage is given by Figure 1

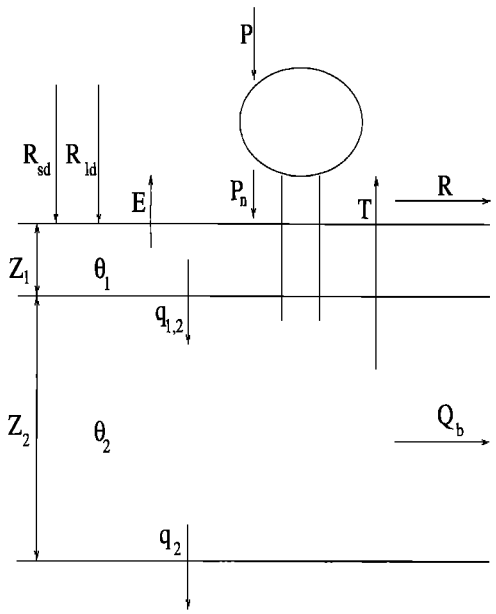

Figure 1. Representation of the thin layer model of soil hydrology.

$$\frac{dC}{dt} = P - P_n$$

$$z_1 \frac{d\theta_1}{\partial t} = P_n - E - R - q_{1,2} \tag{1}$$

$$z_2 \frac{d\theta_2}{\partial t} = q_{1,2} - q_2 - T - Q_b$$

$C(0 \leq C \leq S)$ is the amount of intercepted water on the canopy, S being the canopy storage capacity; the units for S and C are in millimeters; $\theta_1(\theta_r \leq \theta_1 \leq \theta_s)$ and $\theta_2(\theta_r \leq \theta_2 \leq\leq \theta_s)$ are the volumetric soil moistures of layer 1 (with thickness z_1) and layer 2 (with thickness z_2), $q_{1,2}$ and q_2 are the exchange fluxes from layer 1 to layer 2 and drainage from layer 2; roots are present in the bottom layer and extract moisture for transpiration from layer 2 only, T is the transpiration assumed to come out of layer 2 only, R is the runoff, and P_n is the net precipitation reaching the soil surface, which is given by $P_n = P - S_a$, if $P \geq S_a$, where P is the precipitation, and $P_n = 0$ if $P < S_a$, where S_a is the available storage in the canopy given by $S_a = S - C$. The initial conditions for the above set of differential equations is given by $C(t = 0) = C°$, $\theta_1(t = 0) = \theta_1^\circ$, and $\theta_2(t = 0) = \theta_2^\circ$. The water table is assumed to lie below the bottom layer, and the dynamics of the water table are not modeled. Also, the capillary rise from the water table is not considered. Since the object of this study is to simulate the top 1 cm layer soil moisture, it is assumed that the changes in the depth of the water table do not affect the top layer soil moisture. However, when the water table is close to the surface (such as an area adjacent to a stream channel), this assumption will break down. The model is not being used at a

fine spatial resolution to simulate the soil moistures close to stream channels; it is used for a catchment in an average sense.

The parameters in the following paragraph deal with the soil-vegetation system which is built on the physics to capture the diurnal cycle of the land surface response to atmospheric forcings. The soil hydraulic parameters deal with the movement of moisture in the soil; the soil thermal properties characterize the soil surface interaction with long and shortwave radiation. The vegetation parameters determine the amount of transpiration and the base flow parameters help in estimating the runoff at the catchment outlet. The incoming radiation (shortwave and longwave) is computed using Beer's law attenuation to the observations at the top of the canopy [*Choudhury et al.*, 1988] using the extinction coefficient of 0.35 for grasses [*Eagleson*, 1982; *Larcher*, 1975]. The aerodynamic resistances for the transfer of moisture and heat follows that of *Brutsaert* [1982]. The potential evaporation from bare soil, potential evaporation from the canopy storage, and the potential transpiration of the canopy is computed using energy balance [*Famiglietti et al.*, 1994a; *Lakshmi*, 1995]. The actual evaporation from bare soil (E) is controlled by the soil hydraulic properties, conductivity and diffusivity [*Mahrt and Pan*, 1984]. The soil conductivity and diffusivity are computed using the Brooks-Corey relations [*Brooks and Corey*, 1964] and the parameters corresponding to the appropriate soil types [*Rawls et al.*, 1982]. The actual transpiration (T) of the vegetation is a function of the potential, soil moisture of the lower layer, wilting point, and a transition point which serves as a switch between potential and soil controlled [*Neghassi*, 1974]. The actual evaporation from the canopy storage depends on the ratio of the amount of moisture in the storage and its capacity and the potential evaporation [*Rutter et al.*, 1975]. The storage capacity (S in millimeters) is related to leaf area index (L) [*Dickinson*, 1984; *Sellers et al.*, 1986] by $S = 0.2L$ [*Dickinson*, 1984]. Leaves covered with a film of water (having intercepted water on them) are assumed not to transpire [*Rutter et al.*, 1975]. The exchange of soil moisture between the top layer and the lower layer ($q_{1,2}$) is governed by gravity (soil conductivity) and the soil moisture gradient (soil diffusivity). The soil conductivity and diffusivity is computed using the greater of θ_1 and θ_2, i.e., where the soil moisture movement originates [*Mahrt and Pan*, 1984]. The drainage from the lower layer (q_2) is the conductivity of the lower layer. The overland runoff (R) is the sum of the infiltration excess and the saturation excess. The infiltration excess is decided by the infiltration capacity dependent on the soil hydraulic properties: conductivity and diffusivity times the soil moisture gradient between the surface and the top layer [*Mahrt and Pan*, 1984]. The saturation excess is the difference between the soil moisture and the saturation soil moisture for the case when the soil moisture of the top layer exceeds the saturation value. There is no surface runoff or infiltration when the air temperature is less than 273 K, as the precipitation is considered to be in the form of snow. The subsurface flow from the lower layer (Q_b) constitutes the base flow and is expressed using the ARNO nonlinear flow equations [*Francini and Pacciani*, 1991; *Liang et al.*, 1994]. After the water balance is computed, the energy balance is resolved to yield the temperatures of the bare soil surface, vegetation and the composite of the soil, and vegetation canopy. For complete details regarding the hydrological model, the reader is referred to *Lakshmi* [1995].

3. Canopy Radiative Transfer Model

The radiative transfer model for the vegetation canopy is a part of the coupled soil-canopy-atmosphere model used in the brightness temperature simulations as well as in the sensitivity studies examining the role of heterogeneities on brightness temperatures. The canopy radiative transfer model described in this section follows the description of *Choudhury et al.* [1990]. The land surface hydrological model (described above) computes the soil moisture and surface temperature of a 1 cm layer, which serves as the bottom boundary conditions for the canopy radiative transfer model. The microwave radiation originating from the soil surface is modulated by the overlying vegetation canopy, resulting in the canopy-top brightness temperature values. This canopy-top brightness temperature (microwave radiance) is attenuated by the atmospheric water vapor before it reaches the satellite sensor.

The soil-canopy temperature T_0 and the top layer soil moisture θ_1 are used in the canopy scattering model [*Choudhury et al.*, 1990] to compute the canopy-top horizontally and vertically polarized brightness temperatures.

The radiative transfer model treats the interaction of microwave radiation from the soil with the vegetation branches, stems, and leaves. The model is based on a high-frequency approximation: the extinction cross section area of the scatterer equals their geometrical shadow area. The model also assumes that there is no transmission of radiation by the stems and the branches. All radiation on the stems and branches is absorbed. The model is analytic and provides an expression for the canopy-top brightness temperature using the two-point Gaussian quadrature, which results in a system of two coupled ordinary differential equations with the bottom boundary condition dictated by the soil moisture and soil-canopy temperature and the top boundary condition dependent on the radiation from the sky incident on the canopy. This microwave radiation is then attenuated by the atmospheric water vapor before it reaches the satellite.

The canopy-top brightness temperature $T_B(\gamma, p)$ is related to the at-satellite brightness temperature $T_B(A, \gamma, p)$ for zenith angle γ of the sensor, polarization p (horizontal or vertical), and A (the altitude of the radiometer) by

$$T_B(A, \gamma, p) = \tau_a(A, \gamma)T_B(\gamma, p) + T_{\text{atm}}(A, \gamma) \qquad (2)$$

where $\tau_a(A, \gamma)$ is the transmissivity of the atmosphere, and $T_{\text{atm}}(A, \gamma)$ is the radiation entering the radiometer from the atmosphere.

The canopy-top brightness temperature $T_B(\gamma, p)$ will be derived followed by the derivation and discussion of $\tau_a(A, \gamma)$ and $T_{\text{atm}}(A, \gamma)$. The radiative transfer equation is given by [*Choudhury et al.*, 1990; *Stephens*, 1988] as

$$\mu \frac{dI(x, \mu)}{dx} = k(\mu)\left[-I(x, \mu) + \frac{\omega(\mu)}{2} \cdot \int_{-1}^{1} P(\mu, \mu')I(x, \mu')\, d\mu' + (1 - \omega(\mu))T_0 \right] \qquad (3)$$

where $I(x, \mu)$ is the radiance at depth x within the canopy (the top of the canopy is taken as $x = 0$, and the bottom of the canopy is taken to be $x = 1$) at an angle whose cosine is μ ($\mu = \cos(\gamma)$, $\mu > 0$ for radiation direction toward soil and $\mu > 0$ for radiation direction away from soil), $k(\mu)$ is the

extinction coefficient, $\omega(\mu)$ is the single-scattering albedo, $P(\mu, \mu')$ is the phase function (the probability that the element will scatter incident radiation at μ' to direction μ), and T_0 is the soil-canopy temperature.

The boundary conditions are given by

$$I(0, \mu) = T_{\text{sky}}$$
$$I(1, -\mu) = R(\mu)I(1, \mu) + (1 - R(\mu))T_0 \quad (4)$$

where T_{sky} is the intensity of atmospheric radiation incident on the top of the canopy and $R(\mu)$ is the reflectivity of the soil. The first condition states that the downwelling radiation at the top of the canopy is the sky radiation, and the second condition states that the upwelling radiation at the bottom of the canopy equals the emissivity of the soil plus the incident radiation reflected at the soil surface.

The canopy-top brightness temperature is given by

$$T_B(\gamma, p) = I(0, -\mu) \quad (5)$$

The above differential equation is solved by using the two-point Gaussian quadrature [*Chandrashekar*, 1960] to yield the brightness temperatures. The brightness temperature is given by a linear combination of T_{sky} and T_0 as

$$T_B(\gamma, p) = AT_{\text{sky}} + (1 - A)T_0 \quad (6)$$

where A is defined as the effective reflectivity of the soil-canopy system [*Choudhury et al.*, 1990]. The polarization difference index is defined as the difference between the horizontally polarized and the vertically polarized reflectivity of the soil-canopy system [*Lakshmi*, 1995]. For details regarding the derivation of the brightness temperatures, the reader is referred to *Choudhury et al.* [1990] or *Lakshmi* [1995]. The polarization difference index is a better estimate of soil moisture than the polarization difference of brightness temperatures since it does not depend on surface temperature, air temperature, or precipitable water used to compute satellite brightness temperature. The values of the polarization difference index are multiplied by 100 in all figures, tables, and discussions. This is done for the sake of convenience in the interpretation of the numerical results and does not change the results in any way.

4. Atmospheric Attenuation Model

The canopy-top brightness temperatures undergo atmospheric attenuation due to atmospheric oxygen and water vapor before resulting in the at-satellite brightness temperatures ($T_B(A, \gamma, p)$). The optical thickness is computed on the basis of the total precipitable water vapor in the atmospheric column V (in millimeters) [*Choudhury*, 1993] and is related to the atmospheric transmissivity (τ_a). The effective radiating temperature of the atmosphere is related to the air temperature T_a and the total precipitable water. The total precipitable water and the effective radiating temperature are used to compute the sky temperature T_{sky}, which serves as the upper boundary condition on the canopy. The at-satellite brightness temperature ($T_B(A, \gamma, p)$) is computed using the canopy-top brightness temperatures ($T_B(\gamma, p)$) for polarization p (horizontal or vertical), altitude A, atmospheric attenuation $\tau_a(A, \gamma)$, and atmospheric radiation entering the radiometer $T_{\text{atm}}(A, \gamma)$ (approximated to be equal to T_{sky}) [*Ulaby et al.*, 1981] as

$$T_B(A, \gamma, p) = \tau_a(A, \gamma)T_B(\gamma, p) + T_{\text{sky}} \quad (7)$$

The average ($\bar{T}_B$) and polarization difference (ΔT) brightness temperature are defined as

$$\bar{T}_B = \tfrac{1}{2}[T_B(A, \gamma, V) + T_B(A, \gamma, H)]$$
$$\Delta T = T_B(A, \gamma, V) - T_B(A, \gamma, H) \quad (8)$$

5. Hydrological Model Testing and Validation

This section describes the application of the thin layer hydrological model on a catchment for simulation of water and energy fluxes. The description of the catchment, the sources of the data, the calibration of the parameters, and the validation of the results using observed data are described below.

5.1. Site Description

The purpose of the modeling effort was to carry out a 10 year simulation over the Kings Creek catchment along with validation. The First International Satellite Land Surface Climatology Project (ISLSCP) Experiment (FIFE) was a land-surface–atmosphere experiment carried out on a 15 × 15 km site near Manhattan, Kansas [*Sellers et al.*, 1992]. This area is covered by tallgrass prairie, and it consists of rolling hills. The goals of the experiment (as outlined by *Sellers et al.*, [1992]) were to carry out upscale integration of models from a plant scale to a scale amenable to the use of remotely sensed satellite data and to test applications of satellite data and validate hydrological models of land surface processes. The hydrological model described above is applied to the 11.7 km^2 Kings Creek catchment located in the northwestern corner of the FIFE site. The field experiment was carried out in four distinct durations (termed as IFCs (Intensive Field Campaigns)) during IFC-1 (June 1–6, 1987), IFC-2 (June 25 to July 11, 1987), IFC-3 (August 6–21, 1987), and IFC-4 (October 5–16, 1987). The simulated surface soil moistures and temperatures are compared with the observations during these periods on an hourly basis.

5.2. Data and Parameters

The hourly meteorological data corresponding to Topeka, Kansas, are taken from Earth Info's NCDC (National Climate Data Center) Surface Airways data product. The variables used here from that database are air temperature, dew point temperature, air pressure, wind speed, cloud height (defined as the height of the lowest sky cover layer more than one-half opaque), total sky cover, and wind speed. The 10 year (1980–1989) hourly rainfall data were obtained from the Tuttle Creek rain gauge. The rainfall data for the duration of the FIFE IFCs were obtained from the FIFE Information System (FIS) and used in the simulations. The same was the case for the meteorological data for the periods during the Intensive Field Campaigns where observed data were available for Kings Creek; those data were used in place of the Topeka Surface Airways data. The incoming shortwave radiation is modeled using the two-stream approach outlined by *Dubayah et al.* [1990] and *Dubayah* [1992]. It is corrected for cloud cover effects using an empirical correction factor $1 - (1 - K)N$, where $K = 0.18 + 0.0853z$, z is the cloud base altitude in kilometers and N is the fraction of sky covered with clouds [*Eagleson*, 1970]. The incoming longwave radiation is given by $\varepsilon_a \sigma T_a^4$, where ε_a is the clear sky atmospheric emissivity dependent on atmospheric water content [*Idso*, 1981] given by $\varepsilon_a = 0.74 + 0.0049e$ [*Bras*, 1990] and e is the vapor pressure in millibars,

Table 1. Parameters for the Thin Layer Hydrological Model

Parameter	Value
Albedo (soil), α_s	0.15
Albedo (vegetation), α_v	0.20
Emissivity (soil), ε_s	1.00
Emissivity (vegetation), ε_v	1.00
Roughness length (soil), $z_{0,s}$	0.001 m
Roughness length (vegetation), $z_{0,s}$	0.07 m
Zero plane displacement (soil), d_s	0.0
Zero plane displacement (vegetation), d_v	0.25 m
Top layer thickness, z_1	0.01 m
Bottom layer thickness, z_2	0.99 m
Leaf area index, L	biweekly LAIs
Minimum stomatal resistance, $r_{\min}^{st}$	100 s/m
Porosity, θ_s	0.50
Residual Soil Moisture, θ_r	0.02
Brooks Corey Parameter, m	0.2
Air entry suction head, ψ_c	0.2 m
Saturated hydraulic conductivity, K_s	1.89×10^{-6} ms^{-1}
Transition soil moisture, θ^*	0.12
Wilting soil moisture (volumetric), θ_w	0.05
Meteorological data	hourly data, Topeka, Kansas
Rainfall data	hourly data, Tuttle Creek
Streamflow data	daily, Kings Creek

T_a is the air temperature, and σ is the Stefan-Boltzmann constant. The incoming longwave radiation is corrected for cloud effects using the fraction of cloud cover N as $1 + 0.17\ N^2$ [*Tennessee Valley Authority (TVA)*, 1972]. The data for the air temperature, vapor pressure, cloud cover, and cloud base altitude are obtained from the Earth Info Surface Airways data set for Topeka, Kansas.

The vegetation data have been obtained from the University of Maryland reprocessed NOAA global vegetation index (GVI) data product [*Goward et al.*, 1994]. This NOAA GVI has been put together from measurements made by the advanced very high resolution radiometer (AVHRR) onboard NOAA polar orbiting satellites. The data comprises three years (1983, 1987, and 1989) of biweekly composite observations. The leaf area index is computed using the normalized difference vegetation index (NDVI) using a Beer's law kind of variation [*Baret and Guyot*, 1991]. The values of the leaf area index for the years other than 1983, 1987, and 1989 are taken as the average of the values from 1983, 1987, and 1989 data. Missing periods embedded in the 1983, 1987, and 1989 data are estimated by simple interpolation. The resolution of the NDVI GVI is about 16 km at the equator. The other data used in this study have been tabulated in Table 1.

The soil type at Kings Creek is silt loam. The values of the residual and saturated volumetric soil moisture contents are taken to be 0.02 and 0.50, respectively; the Brooks-Corey parameter is equal to 0.2; the air-entry suction head is 0.20 m; and the saturated hydraulic conductivity for silt loam is 6.8 mm/h [*Rawls et al.*, 1982]. The albedo of bare soil and vegetation is taken as 0.15 and 0.20; the emissivity of bare soil and vegetation are taken to be unity [*Famiglietti et al.*, 1994a]. The zero plane displacement for bare soil and vegetation are zero and 25 cm, respectively; the roughness lengths for bare soil and vegetation are 1 mm and 7 cm, respectively. The average daily air temperature computed using the Earth Info data set is taken to be the soil temperature at 5 cm depth (for use in ground heat flux calculation). The initial interception storage is taken to be zero. The values of the transition and wilting volumetric soil moisture contents are 0.12 and 0.045. The minimum stomatal resistance is equal to 100 s/m. The base flow parameters for the ARNO model $Q_b^{\max}$, θ_b^*, and Q_b^* [*Francini and Pacciani*, 1991] and the exponent Λ in the transpiration relationship [*Neghassi*, 1974] are calibrated using the observed daily flows at Kings Creek U.S. Geological Survey stream gauge data.

5.3. Results and Discussions

The hydrological model described in the previous sections is used to simulate the water and energy fluxes for the Kings Creek catchment for a period of 10 years (1980–1989) on a hourly time step. The parameters are calibrated using the first 5 years (1980–1984), and the validation is done for the 1985–1989 streamflows. The calibrated parameter values are used to generate the streamflows, soil moistures, and surface temperatures at an hourly time step for the entire 10 year period. The soil moistures for the time period corresponding to the four Intensive Field Campaigns (IFCs) in FIFE 1987 are compared. There has been no adjustment or initialization of the soil moistures at the start of the IFCs.

Calibration and validation of streamflows. The hourly streamflows are simulated over the first 5 year period (1980–1984) and aggregated to daily values. The parameters are optimized using the root-mean-square of the difference between the observed flows (obtained using the daily discharge values at Kings Creek) and the simulated values over the 5 year period. This results in the values of $Q_b^{\max}$, θ_b^*, Q_b^* (ARNO model), and Λ (transpiration parameter) as 3.38 mm/h, 0.15, 0.06 mm/d, and 0.50, respectively. The root-mean-square of the error of the streamflow over the 1980–1984 period is 1.7 and 1.6 mm over the 1985–1989 period (see Figures 2 and 3). The variations of the daily averaged simulated volumetric soil moisture for the top and bottom layers are shown in Figure 4. The results of the streamflow calibration and validation are plotted as time series for 1980–1984 and 1985–1989 in Figures 2 and 3, respectively. The agreements between the simulated (solid lines) and the observed streamflows (dotted lines) at the Kings Creek gauging station are reasonable. The disagreements could be due to the use of rainfall data from the Tuttle Creek rain gauge which is about 20 km from the FIFE site (caused by the nonavailability of the hourly rainfall data at the Manhattan rain gauge for the period under study). In general, the simulated streamflow overestimates the observed streamflow, but it shows good qualitative agreement. Since the objective of the study is not to match the simulated and the observed runoffs but to simulate a realistic variation of the top soil layer moisture, the streamflow results are acceptable. In the case of the calibration time period (Figure 2) it can be seen in the year 1982 (June 24 and July 1, Julian days 175 and 182, respectively) that the observed streamflows are 8.6 and 50.3 mm, respectively. On examination of the rainfall records of the Tuttle Creek gauge there is no rain between June 16 (Julian day 167) and June 25, 1982 (Julian day 175), and the total rain on July 1, 1982, is 7.8 mm (there is no rain on June 28, 29, and 30, Julian days 179–181). This shows that the rain gauge at Tuttle Creek does not record the storm that results in these large streamflows. The other plots in Figure 2 show better agreement. The same is the case in Figure 3. Figure 4 is the counterpart of Figure 3 giving soil moistures. The observed streamflow on May 17, 1986 (Julian day 137), is 18.1 mm, and there is no rainfall observed at the rain gauge between April 28 (Julian day 118) and May 31, 1986 (Julian day 151). On the

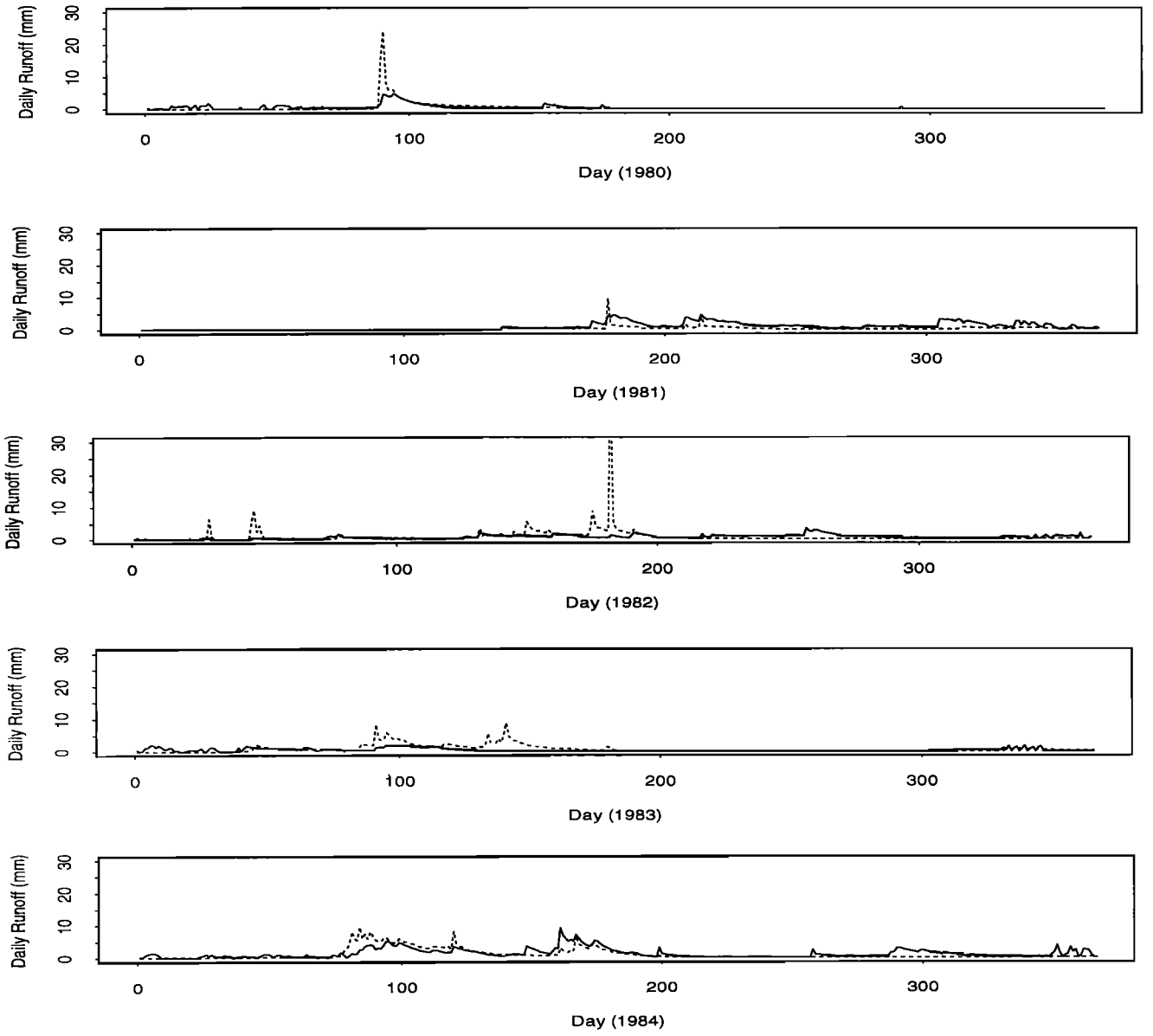

Figure 2. Observed (dotted line) and simulated (solid line) daily discharges (in millimeters) for the calibration period (1980–1984).

other hand, between August 20 (Julian day 232) and October 1, 1989 (Julian day 274), there is a huge overestimation of the streamflow. This is because of a very large base flow estimation that results from the increase in soil moisture of the bottom layer due to 297 mm of rain that is recorded by the rain gauge (see Figure 4). The increase in the bottom layer soil moisture causes increased simulated streamflow (compared to observed streamflow) in the second half of 1986 (from Julian day 200 to 300). The top layer soil moisture shows much greater daily variability than the bottom layer soil moisture. This is consistent with the expected dynamics. In addition there is a greater number of increases in the top layer soil moisture in 1987 where the simulated streamflow is greater than zero for most of the year. This is also the case for the increased number of streamflow events from Julian day 200 to 300 in 1986. In summary, the hydrological model estimates the streamflow with reasonable accuracy as consistent with the rainfall data.

Soil moisture comparisons. The average of the soil moistures observed over the Kings Creek catchment (obtained using the FIFE Information System, FIS database) is plotted against the simulated soil moisture for IFC-1 through 4 for both the top (Figure 6) and the bottom (Figure 7) layers. The observations are made at a depth of 25 and 75 mm at the Bowen ratio stations (2, 8, 10, 12, and 14 corresponding to grid numbers 1916, 3129, 3414, 2915, and 2516). At each station, there are five measurements of soil moisture corresponding to the center, north, south, east, and west (distance approximately 30 m in each case). These are averaged to obtain the catchment averaged soil moisture for comparison with the simulated soil moisture. The simulated soil moistures correspond to a top layer of 10 mm (1 cm) thickness and a bottom layer of 990 mm (99 cm) thickness. The 25 mm observed soil moistures are plotted against the top layer simulated soil moisture, and the 75 mm observed soil moistures are plotted against the bottom

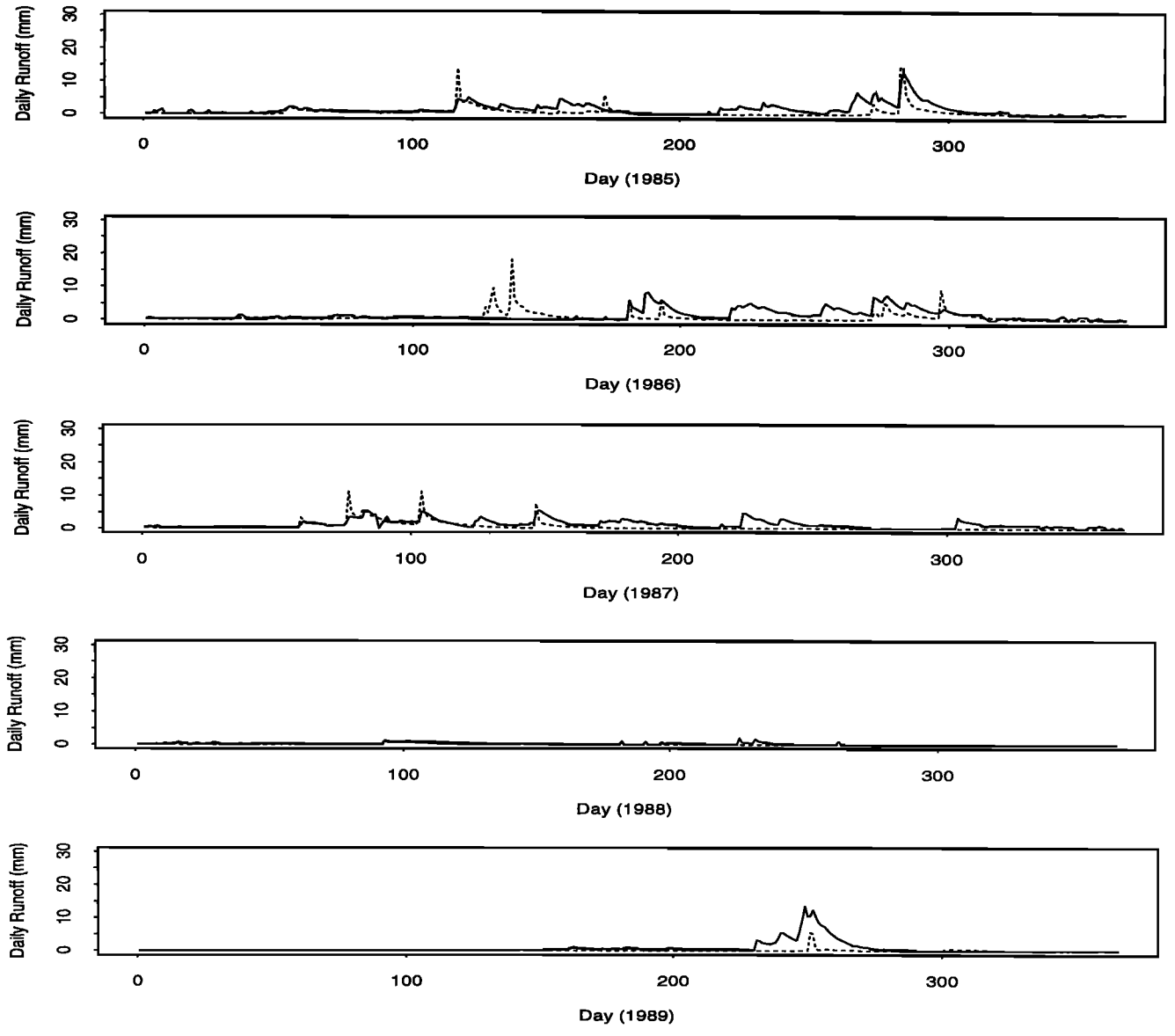

Figure 3. Observed (dotted line) and simulated (solid line) daily discharges (in millimeters) for the validation period (1985–1989).

layer simulated soil moisture. The observed soil moistures are plotted individually at the beginning of the day (i.e., if the observations are on Julian day 152, June 1, 1987, they are plotted corresponding to hour 1, day 152) since the time of day at which the observations are made is not available. Also, the observations are made once daily and do not capture the temporal dynamics of the soil moisture variation. The temporal variation is reflected in the simulated soil moisture. However, note that the abscissa (in days) is over a range of 6 days for IFC-1, 17 days for IFC-2, 16 days for IFC-3 and 12 days for IFC-4. Therefore temporal variations will appear emphasized in IFC-2 and 3 and appear much more gradual in IFC-4 and IFC-1.

The four panels in Figure 6 are for IFC-1 through IFC-4. It is interesting to note that each of them displays different nuances associated with soil moisture dynamics. In the case of IFC-1, there is virtually no rainfall as seen from the rainfall data for the IFCs in Figure 5 (only one hour with 0.2 mm of rain on June 2 at 0900). The observed soil moisture exhibits a very slow decrease (drydown) over time. The simulated soil moisture remains relatively constant for the duration of the IFC. This is because there is replenishment of the loss in soil moisture (due to bare soil evaporation) of the upper layer by diffusive flux from the bottom layer. The bottom layer holds a larger amount of moisture compared to the top layer (capacity of the top layer is equal to 10 mm $\times$ 0.50 (porosity) = 5 mm; capacity of the bottom layer is equal to 990 mm $\times$ 0.50 (porosity) = 495 mm), and therefore the bottom layer soil moisture shows little decrease when it supplies the top layer with moisture (even if there is a 5 mm flux of moisture from the bottom layer to the top layer, the bottom layer soil moisture content decreases by only 0.005). In the case of IFC-2, there is no rainfall on June 25 and 26 (Julian days 176 and 177), and the top layer soil moisture shows a decrease. There is rainfall on June 27, and the soil moistures increase. On June 27 at 2200 there is a 9.65 mm rainfall, and the top layer soil moisture

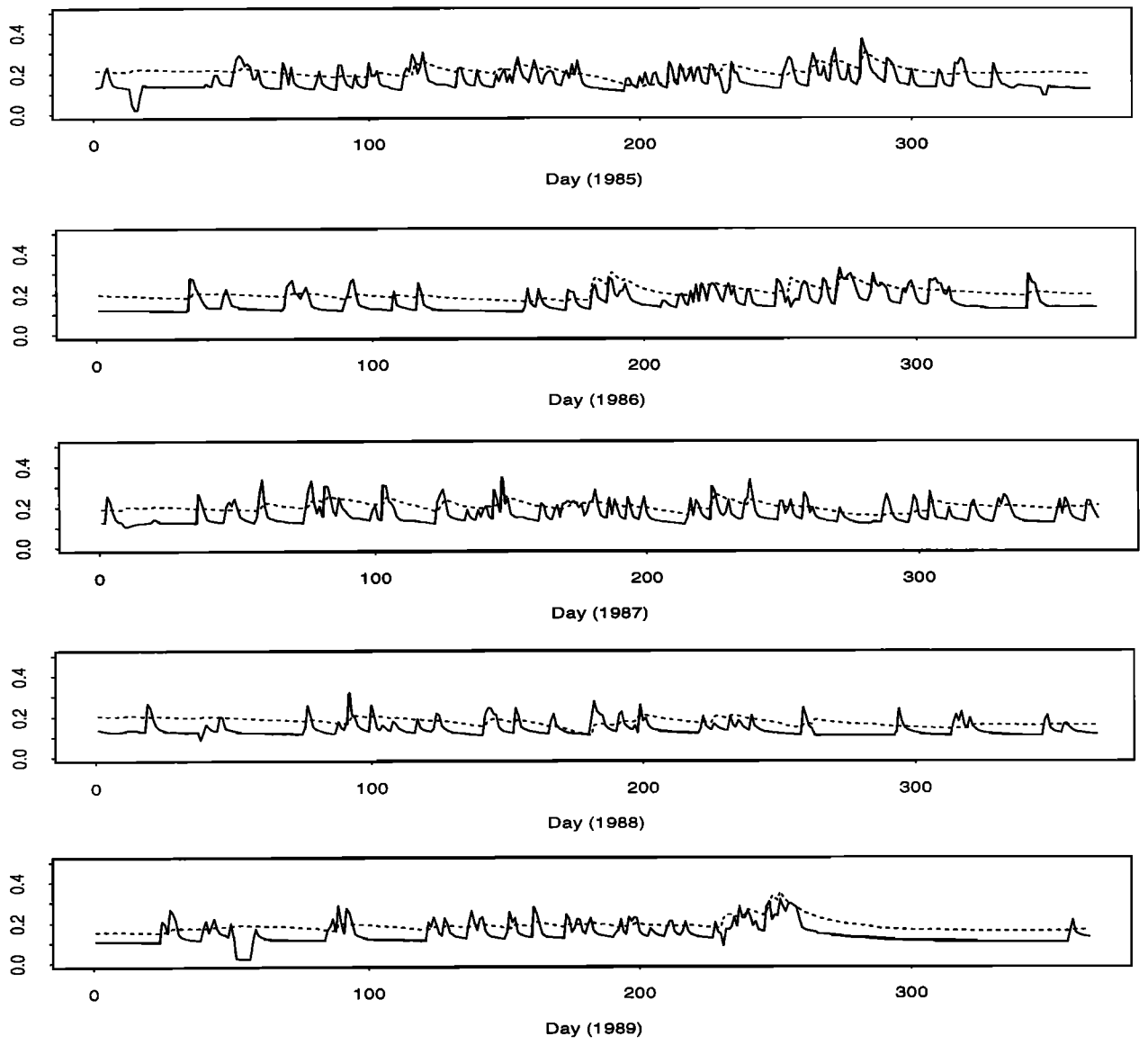

Figure 4. Simulated top layer (solid line) and bottom layer (dotted line) daily averaged soil moisture for 1985–1989.

increases from 0.135 to 0.401. This is expected since the rainfall wets the top layer of the soil almost instantly. The total rainfall on June 27 is 30.98 mm. This rainfall is reflected in the observed 25 mm soil moisture the next day (June 28), which increases from 0.22 on June 27 to 0.31 on June 28. There are two important observations here. The immediate increase in the 25 mm soil moisture is less than the increase seen in the 1 cm soil moisture. The 25 mm soil moisture shows a more gradual change as opposed to the 1 cm soil moisture. On the other hand, the 1 cm soil moisture responds on much shorter (quicker) timescales. This cannot be completely verified since only daily observations of the 25 mm soil moisture are available. After the top layer gets wet in response to the rainfall input, gravity and the soil moisture gradient between the top layer and the bottom layer results in movement of the moisture to the bottom layer. However, since the bottom layer is 99 cm thick, the increase in soil moisture of the bottom layer due to this incoming soil moisture is very slight, as seen in the second panel of Figure 7. There is rainfall between June 27 (178) to June 30 (181), after which there is no rain for a period of 3 days from July 1 to 3 (182–184). We can observe the drydown in the top layer soil moisture from 0.237 on July 1 to 0.139 on July 4. There are again periods of rain on July 4 (about 0.2 mm) and July 5 (8.9 mm), after which there is no rain till the end of the IFC, and the soil moisture of the top layer exhibits a drydown (there is an hour of 1.5 mm of rain on July 7, hence the spike around day 187). The 25 mm observed soil moisture exhibits behavior that agrees with the rainfall input and the simulated 1 cm soil moisture.

IFC-3 behaves similar to IFC-2 in that there are periods of rain and periods of drydown when the soil moisture decreases. The case for IFC-4 is similar to the ones discussed above. There is no rain between October 5 and 13, but there is rainfall in 2 hours of October 13 and 14. Though this rainfall is very slight (1.27 and 0.51 mm), it does increase the soil moisture of the top layer. The rainfall on October 15 increases the upper

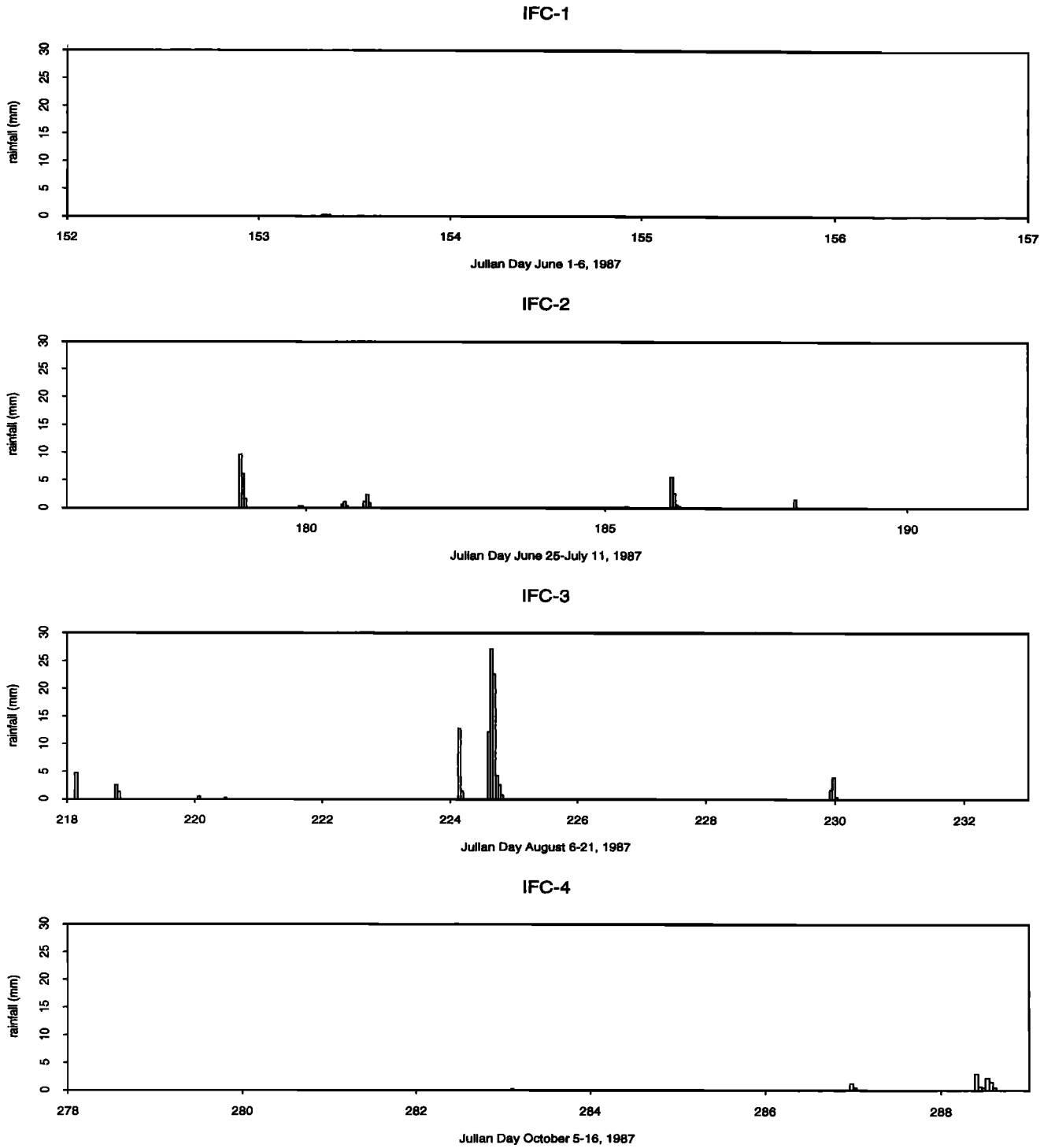

Figure 5. Precipitation (in millimeters) for the Kings Creek gauge for IFC-1 through IFC-4.

layer soil moisture, after which it drops off due to drainage into the bottom layer.

The simulated soil moisture shows consistent agreement with the observed rainfall and the observed 25 and 75 mm soil moistures. Since the top 1 cm layer soil moisture is affected by rainfall almost instantaneously, it is important that the soil moisture accounting scheme operates on hourly time steps (as in the case here) so that the temporal dynamics is captured.

Surface temperature comparisons. The observed hourly surface temperatures from the stations (three super automated mesonet Stations (AMS) 31, 3, and 7) in grid numbers 2123, 2139, 2428, and 3221, respectively, are half hourly observations averaged to hourly values. The observed (dots) and simulated (solid line) are plotted in Figure 8. However, during the mid-day hours the simulated values of surface temperatures are larger than the observed values. The IFC-1 comparisons show

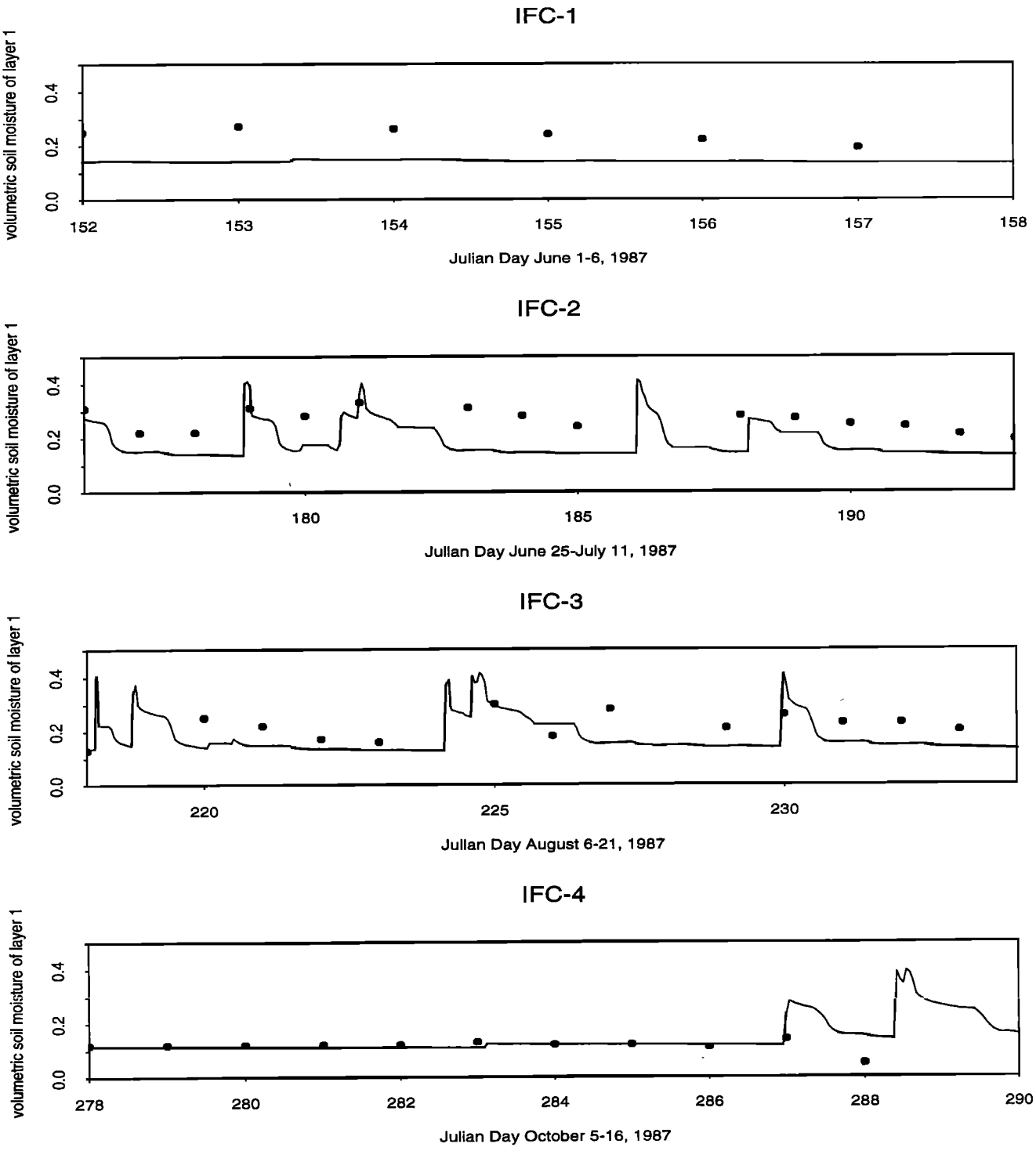

Figure 6. Mean (once a day) observed (25 mm depth, dots) and (hourly) simulated (top layer, lines) volumetric soil moisture for IFC-1 through IFC-4.

reasonable agreements for most of the hours except for a few hours of June 4 (Figure 8) (the fourth peak in panel 1 of Figure 8). There are disagreements between the observed and the simulated surface temperatures of 5 K or more between 1000 and 0600 on that day. The wind speed controls the resistance of the bare soil evaporation and the vegetation transpiration. The aerodynamic resistances are inversely proportional to wind speed. The lower the wind speed, the higher the value of the aerodynamic resistance for bare soil and vegetation. During the day of June 4, 1987, the wind speeds between 1000 and 0600 ranged from 1.4 to 2.1 m/s. This range, when compared to the wind speed variation during the same time on June 5 (4.7 to 11.2 m/s) results in a much larger aerodynamic resistance, thereby reducing the evapotranspiration. It is because of this that the simulated surface temperatures on June 4 show a marked disagreement with the observations. The same expla-

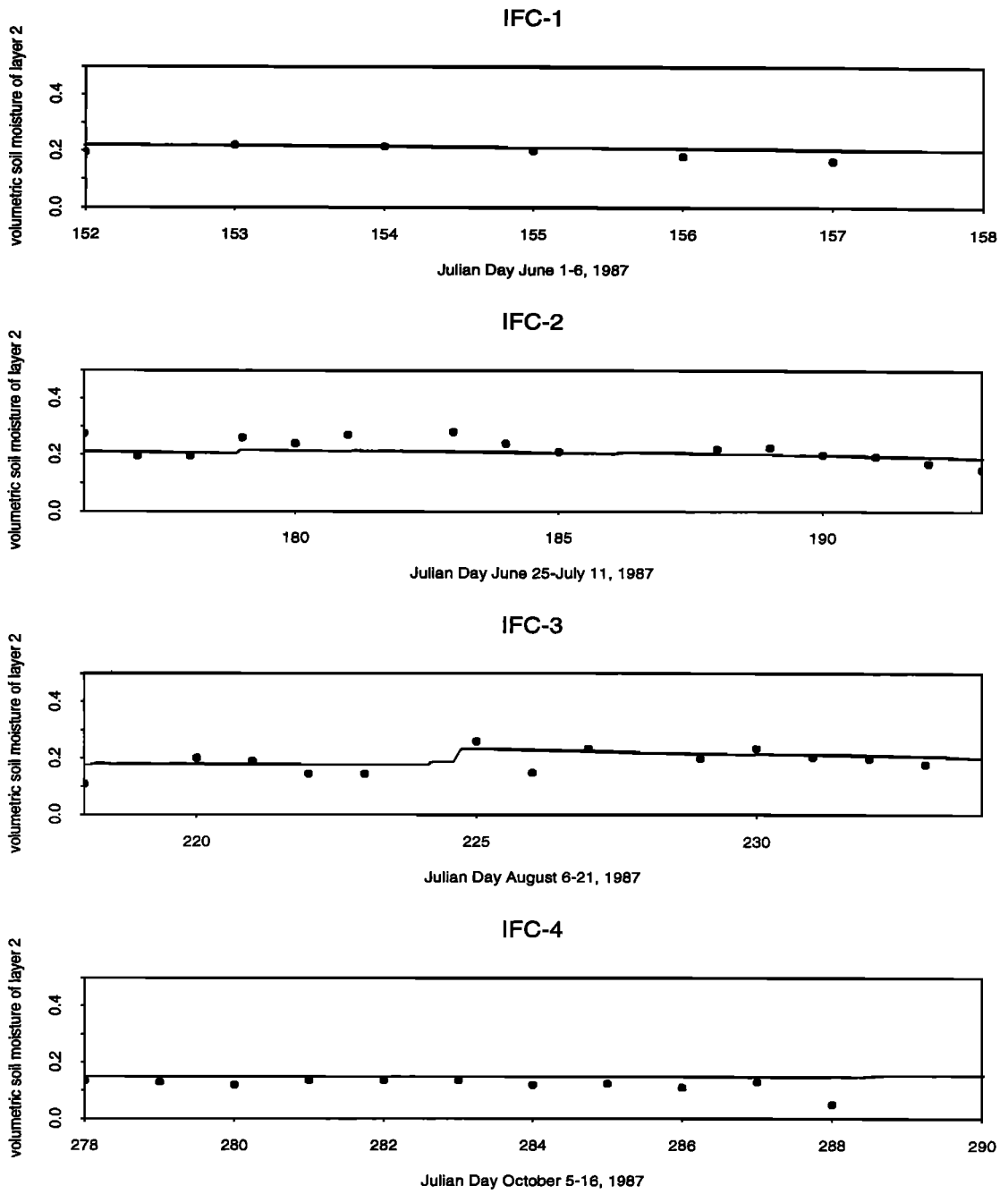

Figure 7. Mean (once a day) observed (average of 25 and 75 mm depth, symbols) and (hourly) sin (bottom layer, lines) volumetric soil moisture for IFC-1 through IFC-4.

nation holds for July 1, 2, and 3 (panel 2, Figure 8); August 10, 11, and 13 (panel 3, Figure 8); and October 11 and 12, 1987 (panel 4, Figure 8). The hours of overestimation coincide with low values of wind speed (which reduce the simulated evapotranspiration) coupled with high values of incoming solar radiation (at midday hours). The high solar radiation (and hence net radiation) results in large values of sensible and ground heat fluxes (since the latent heat is small), and this increases the surface temperature to preserve the energy budget. However, for most part, the simulated surface temperatures do agree well with the observed values. Figure 9 shows the scatter of the simulated surface temperatures with the observed values. The root mean square error over IFC-1 is 5.7 K; IFC-2 is 5.5 K; IFC-3 is 5.9 K; and IFC-4 is 3.6 K. On examining Figure 9, we can observe that there is more overestimation of the observed temperatures than underestimation. The thin top layer could be a factor in the reduced simulated evapotranspiration which results in high midday temperatures.

Since we are especially interested in the 0600 observations, which coincides with the SSM/I ascending orbit overpass, comparisons between the observed and the simulated values at 0600 are meaningful. The root-mean-square error for the 0600 surface temperatures are 1.8, 0.8, 1.5, and 1.2 K for IFC-1, IFC-2, IFC-3, and IFC-4, respectively. The root-mean-square

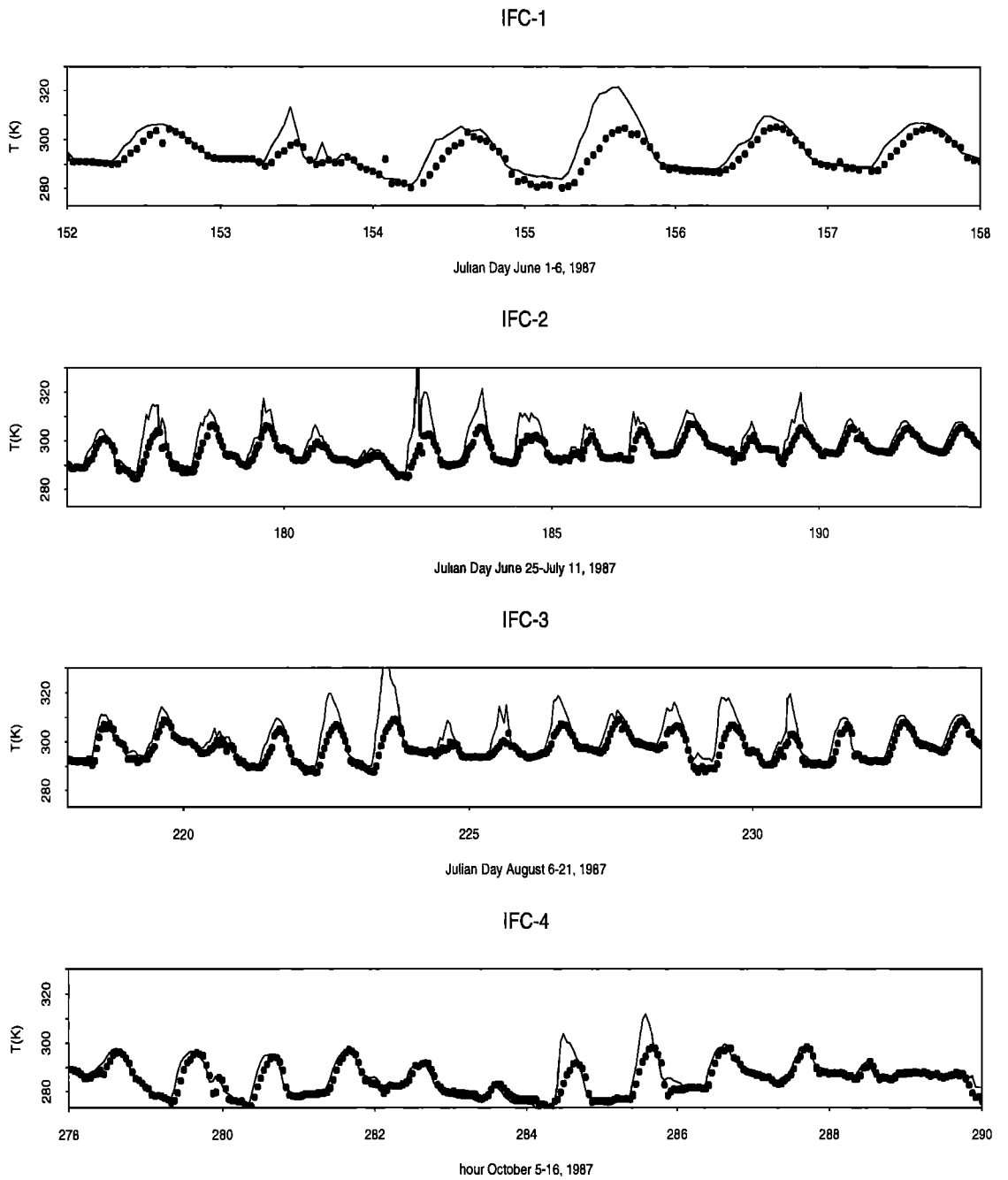

Figure 8. Time series plot of observed hourly surface temperatures (dots) and simulated hourly top layer temperatures (lines) for IFC-1 through IFC-4.

error for all the 0600 surface temperatures lumped together from all the IFCs is 1.3 K. Figure 10 shows the scatterplot between the observed and the simulated 0600 surface temperatures. The agreement is very good.

6. Sensitivity of Radiative Transfer to Vegetation and Soil Moisture

The coupled land surface hydrology-canopy radiative transfer model is used to study the sensitivity of the polarization difference index to changes in leaf area index, soil moisture, and vegetation parameters. The vegetation parameters-stem area index and canopy moisture content are chosen for the sensitivity study as they have the most significant effect on the polarization difference index. These sensitivities will help us in understanding the factors that contribute to the polarization difference index observed by the SSM/I.

6.1. Effect of Vegetation Parameters

The effect of the stem area index (η) and the canopy moisture content (m_c) on the range of the polarization difference index ΔY (X100 as explained earlier; denoted by DY in all figures), the leaf area index (LAI), and the soil moisture range (between residual and saturation) is shown in Figure 11 for the 19 GHz case (a similar variation is seen for the 37 GHz case and is not shown here). The stem area index varies across the

figure panels from 0 to 0.6 from left to right, and the canopy moisture content varies from 0.65 at the top (corresponding to a turgid leaf) to 0.05 at the bottom (corresponding to a dry leaf). The branch to stem area ratio (χ) is set to 2.7, corresponding to the vegetation type shrubs [*Whittaker and Woodwell*, 1967; *Whittaker et al.*, 1974]. The lines drawn in the figures (obtained by simulation) correspond to soil moisture at saturation (the line to the right, i.e., greatest value of DY for a given LAI) and at residual (least value of DY for a given LAI). These lines form the bounding curves in between which values (of ΔY) for other soil moistures lie. The stem area increases and the range between the simulated saturation soil moisture content ΔY and the residual soil moisture content ΔY curves decreases for a given leaf area index. There is a greater decrease in the polarization difference index for the saturation soil moisture than for the residual soil moisture.

The polarization difference signal originates at the soil surface and propagates through the vegetation. This polarization difference signal caused by the bipolar nature of the water molecule is greatest for a saturated soil. The increase in leaf area index and/or stem area index attenuates this signal. This attenuation of the polarization difference index is greater for the saturation soil moisture ΔY curve as opposed to the residual soil moisture ΔY curve for both the increase in leaf area index and the stem area index. At sufficiently high leaf area index (in this case 7.0) the polarization difference index of the residual and the saturation soil moisture curves (for all stem area indices and leaf moisture contents of 0.65 and 0.35) coincide.

Increasing canopy moisture content also decreases the polarization difference signal, as seen from the figures moving bottom to top. When the leaf is dry (m_c = 0.05), the polarization difference index stays high, even at high leaf area indices. Turgid leaves absorb the microwave radiation and polarization difference emitted from the surface of the soil [*Choudhury et al.*, 1990]. Therefore an increase in the canopy moisture content attenuates the polarization difference index. The above observations are common to both 19 and 37 GHz polarization difference indices.

Table 2 shows the variation of the simulated maximum range of the polarization index (ΔY), i.e., the difference between the polarization index for the soil saturated case and the soil dry case for varying the stem area index and the canopy moisture content. As the observations from Figure 11 showed, the range decreases with increasing stem area index and increasing canopy moisture content. Furthermore, the range is greater for the 19 GHz case as opposed to the 37 GHz case, but for a dry leaf (m_c = 0.05), they are almost identical. This shows that the vegetation exerts greater influence in modulating the polarization difference signal for 37 GHz as opposed to 19 GHz. In addition, for the case of a dry leaf and stem area index equal to zero, the polarization difference index is identical (13.0) for both the 19 and the 37 GHz frequency. In this case, there is almost no influence exerted by the vegetation on the polarization difference signal originating from the soil. Hence for the case of zero stem area index and zero canopy moisture content, the polarization difference index for the 19 and 37 GHz differs only due to the difference in the dielectric properties of water, which are a function of frequency (the Fresnel reflectivity is 0.2124 for 19 GHz and 0.209 for 37 GHz for volumetric soil moisture of 0.50) and is small.

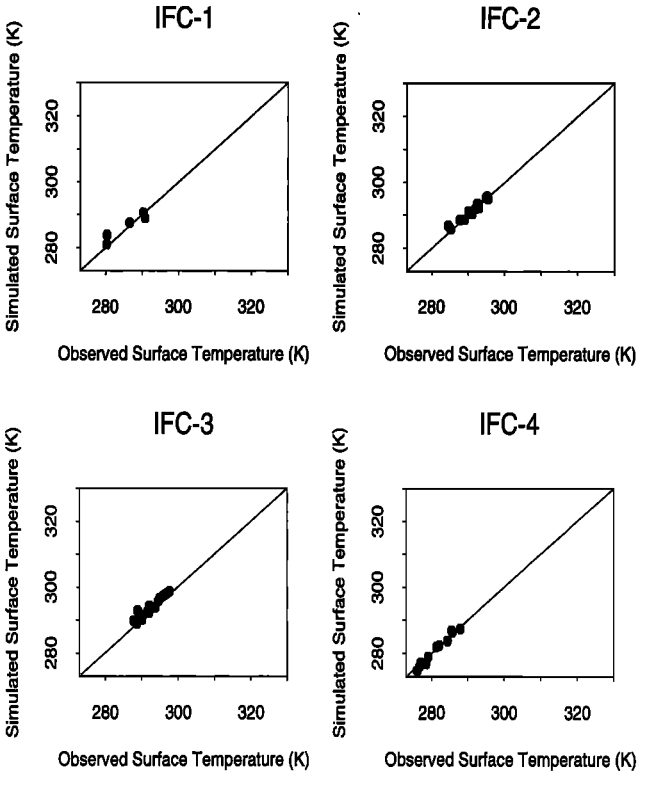

Figure 10. Scatterplot of 0600 observed surface temperatures and simulated top layer temperatures for IFC-1 through IFC-4.

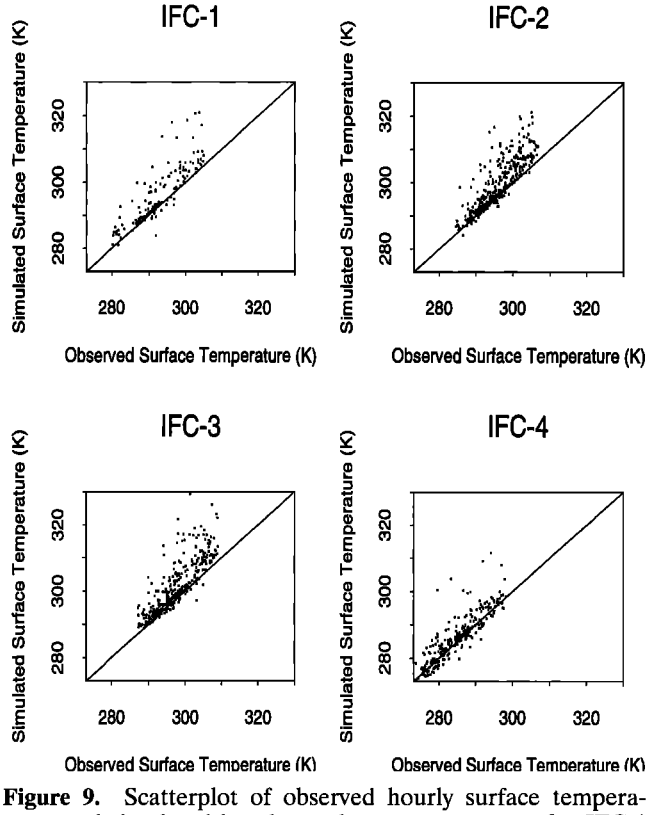

Figure 9. Scatterplot of observed hourly surface temperatures and simulated hourly top layer temperatures for IFC-1 through IFC-4.

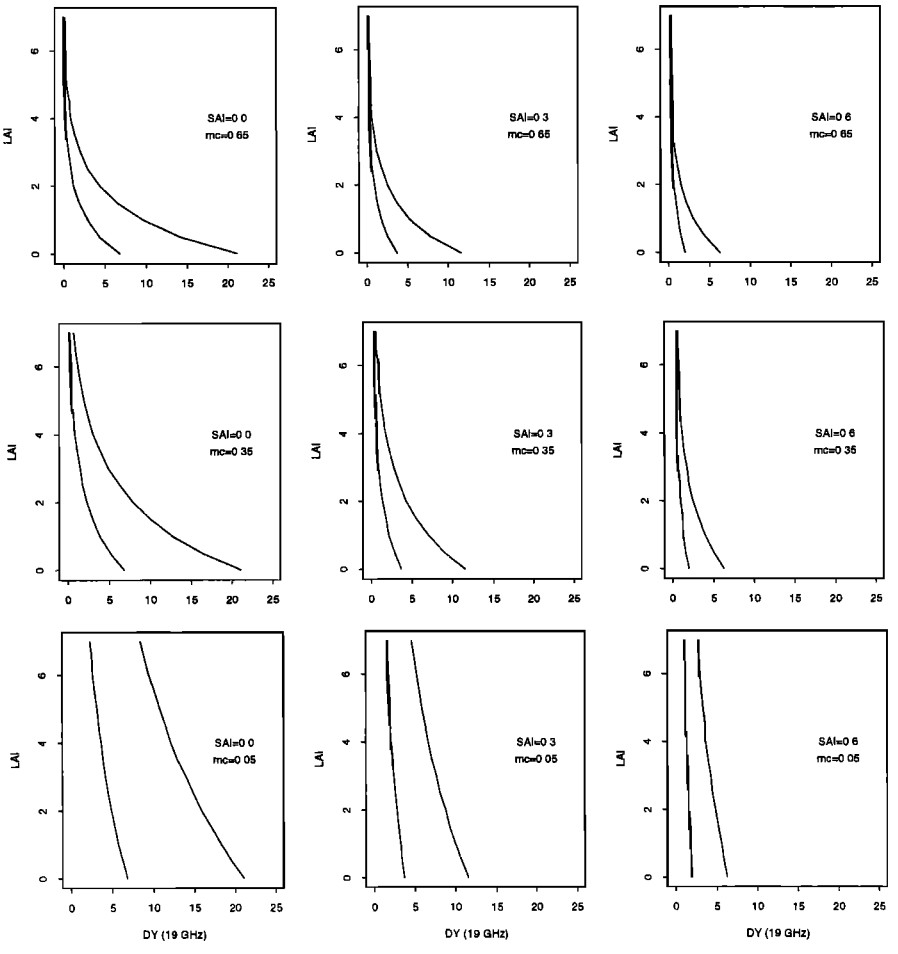

Figure 11. Sensitivity of 19 GHz polarization difference index (DY) to the leaf area index (LAI) for different values of stem area index (SAI) and canopy moisture content (mc).

6.2. Sensitivity to Leaf Area Index and Soil Moisture

Our aim in this section is to show the affect of various biophysical variables on simulated polarization difference indices. The polarization difference indices derived from the SSM/I will be used to ascertain soil moisture values [*Lakshmi et al.*, 1996b]. We are trying to outline the fact that there are sensitivity issues involved in the sensitivity of the polarization difference index: (1) sensitivity with respect to soil moisture for a range of leaf area indices and (2) sensitivity with respect to leaf area index for a range of soil moisture values. The sensitivities of the polarization difference-index ΔY to leaf area index L and soil moisture θ can be expressed as $\partial \Delta Y/\partial L$, and $\partial \Delta Y/\partial \theta$ will both be a function of the vegetation parameters, the stem area index and the canopy moisture content that were examined in the previous section. This section will examine these sensitivities for a stem area index of 0.3 and a canopy moisture content of 0.35.

Table 2. Maximum Simulated Range Residual to Saturated Soil Moisture Content ($\theta_s - \theta_r$) for Polarization Difference Index ($\Delta Y \times 100$) Leaf Area Index (L) = 0.75

Stem Area Index (χ)	Canopy Moisture (m_c)	ΔY (×100) (19 GHz)	ΔY (×100) (37 GHz)
0.0	0.65	8.3	7.3
0.3	0.65	4 4	3.9
0.6	0 65	2.4	2.1
0.0	0.35	10.1	9.4
0.3	0.35	5.5	5.0
0.6	0.35	3.1	2.7
0.0	0.05	13.0	13.0
0.3	0.05	7.1	7.0
0.6	0.05	3.9	3.7

Branch to stem area ratio (η) = 2.7 for 19 and 37 GHz.

The sensitivity of the polarization difference index to the leaf area index $\partial \Delta Y/\partial L$ has to be evaluated at a fixed value of soil moisture. It will be a function of the soil moisture and the leaf area index (in the neighborhood of which it is being evaluated). This can be seen in the top half of Figure 12, in which the variation of polarization difference index for 19 GHz has been plotted against the leaf area index for different values of the soil moisture content ranging from 0.02 (residual) to 0.50 (saturation) for 10 increments, and it can be seen from the figure that as the soil moisture decreases, $\partial \Delta Y/\partial L$ decreases; that is,

$$\theta_1 < \theta_2 \rightarrow \left(\frac{\partial \Delta Y}{\partial L}\right)_{L,\theta=\theta_1} < \left(\frac{\partial \Delta Y}{\partial L}\right)_{L,\theta=\theta_2} \tag{9}$$

In the case of 19 GHz (Figure 12), for $L = 1.0$, $\partial \Delta Y/\partial L$ is 1.1 for $\theta = 0.02$ (residual soil moisture) and 3.5 for $\theta = 0.5$ (for saturation soil moisture). The value of $\partial \Delta Y/\partial L$ is computed

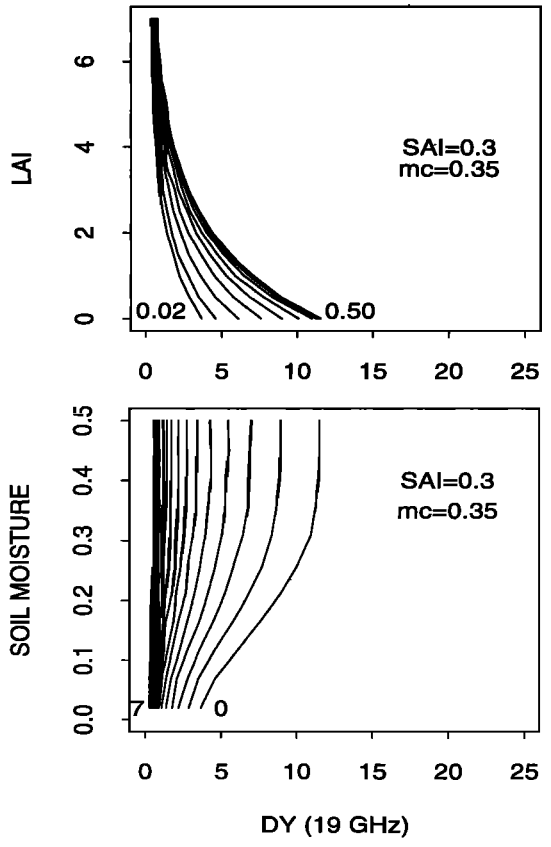

Figure 12. Sensitivity of 19 GHz polarization difference index (DY) to leaf area index for different soil moisture contents between 0.02 (residual) and 0.50 (saturation) and for volumetric soil moisture content for different leaf area indices between 0.0 and 7.0 for stem area index and canopy moisture content at 0.3 and 0.35, respectively.

using the ΔY values for the leaf area index L of 0.5 and 1.5. In the case of θ taking up intermediate values between 0.02 and 0.5, the value of $\partial\Delta Y/\partial L$ lies between 1.1 and 3.5; 1.8 for θ = 0.12; 2.7 for θ = 0.21; and 3.3 for θ = 0.31. In the case of 37 GHz the values are similar but slightly higher for θ = 0.5, $\partial\Delta Y/\partial L$ = 3.6. This shows that the 37 GHz frequency has an increased sensitivity to leaf area index.

The sensitivity to leaf area index of the polarization difference is maximum for the case of saturation soil moisture and minimum for the case of residual soil moisture. Hence we can write

$$\left(\frac{\partial\Delta Y}{\partial L}\right)_{L,\theta=\theta_r} \leq \left(\frac{\partial\Delta Y}{\partial L}\right)_{L,\theta=\theta_1} \leq \left(\frac{\partial\Delta Y}{\partial L}\right)_{L,\theta=\theta_s} \quad \theta_r \leq \theta_1 \leq \theta_s \tag{10}$$

In addition, as the leaf area index increases, the sensitivity to leaf area index decreases (at a fixed value of soil moisture) that is,

$$L_1 < L_2 \rightarrow \left(\frac{\partial\Delta Y}{\partial L}\right)_{L_1,\theta} > \left(\frac{\partial\Delta Y}{\partial L}\right)_{L_2,\theta} \tag{11}$$

Using the above values, for a value of θ = 0.21, the value of $\partial\Delta Y/\partial L$ is 2.7 for L = 1.0; 1.5 for L = 2.0; 0.9 for L = 3.0; and 0.4 for L = 5.0.

However, for higher soil moisture contents, the sensitivity of the polarization difference index to leaf area index still remains significant even when the leaf area index increases. This can be seen in Figure 12, for example, for θ = 0.12, for L = 1.0, $\partial\Delta Y/\partial L$ = 1.8; L = 2.0, $\partial\Delta Y/\partial L$ = 1.0; and for L = 3.0, $\partial\Delta Y/\partial L$ = 0.6 for the 19 GHz case. In the case for θ = 0.31 the corresponding values are 3.3, 1.9, and 1.1 for L = 1, 2, and 3, respectively. So, for the leaf area index of 3, $\partial\Delta Y/\partial L$ is 1.0 for θ = 0.31 but only 0.6 for θ = 0.12. The corresponding values for the 37 GHz case are 1.7, 0.8, and 0.5 for L = 1, 2, and 3, respectively (for θ = 0.12) and 3.3, 1.7, and 1.0 for L = 1, 2 and 3, respectively (for θ = 0.31).

At higher values of leaf area index, the polarization difference signal gets attenuated by the vegetation canopy. The strength of the polarization difference signal is a function of the soil moisture content. At higher soil moisture contents the polarization difference signal does not get completely attenuated at larger values of leaf area index, and therefore there is still sensitivity to the leaf area index. On the other hand, for low soil moisture contents the polarization difference signal is low to begin with and gets attenuated with increasing leaf area index to a degree that further changes in leaf area index do not affect the signal, hence reducing the sensitivity.

The sensitivity of the polarization difference index to the soil moisture $\partial\Delta Y/\partial\theta$ is evaluated at a fixed value of leaf area index. The sensitivity of $\partial\Delta Y/\partial\theta$ is a function of the leaf area index and the soil moisture content in the neighborhood in which it is evaluated. The variation of the polarization difference index with soil moisture for different leaf area index values ranging between 0 and 7 at increments of 0.5 is presented in bottom half of Figure 12. It can be seen that as the leaf area index increases, the sensitivity of the polarization difference to the soil moisture $\partial\Delta Y/\partial\theta$ decreases (for a given θ); that is,

$$L_1 < L_2 \rightarrow \left(\frac{\partial\Delta Y}{\partial\theta}\right)_{L=L_1,\theta} > \left(\frac{\partial\Delta Y}{\partial\theta}\right)_{L=L_2,\theta} \tag{12}$$

The value of the 19 GHz $\partial\Delta Y/\partial\theta$ for θ = 0.12 is 31.25 for L = 0; 17.7 for L = 1.0; 11.5 for L = 2.0; and 4.2 for L = 4.0. It can be seen that as the leaf area index increases, the sensitivity rapidly decreases. This is expected since increasing leaf area index masks the polarization difference signal of the soil moisture. The 37 GHz $\partial\Delta Y/\partial\theta$ also behaves similarly. The values of $\partial\Delta Y/\partial\theta$ are 22.9, 10.4, 6.25, and 1.0 corresponding to L of 0, 1.0, 2.0, and 4.0, respectively, for θ = 0.12. It can be seen that the sensitivity values of $\partial\Delta Y/\partial\theta$ are lower for the 37 GHz than for the 19 GHz. This is expected, as the 19 GHz has greater sensitivity to the soil moisture due to its longer wavelength. The decrease of $\partial\Delta Y/\partial\theta$ with leaf area index results in almost zero sensitivity when high values of leaf area index (like L = 7.0) are approached. This can be seen in Figure 12; the ΔY versus θ curve for L = 7.0 is almost a straight vertical line. As the soil moisture increases from residual soil moisture content, $\partial\Delta Y/\partial\theta$ first increases and then decreases. This can be seen by observing the slope $\partial\Delta Y/\partial\theta$ of the ΔY versus θ curve (for a fixed L). As the soil moisture increases (for a given leaf area index), the sensitivity of the polarization difference to the soil moisture increases. After a certain soil moisture content, the polarization difference signal gets saturated, and further increases in soil moisture do not result in corresponding increases in polarization difference index. The results for the 37 GHz case show similar variations. The figure for the 37 GHz

case is not shown here because the results for 37 GHz qualitatively resemble that for 19 GHz and has no new features.

7. Conclusions

A thin layer model of hydrology with complete water and energy budgets has been presented here. The model is built on the framework of *Mahrt et al.* [1984] for inclusion of a thin upper layer. The parameterizations include the moisture gradient driven flux for diffusion of water from the lower layer to the upper layer to replenish the moisture lost during evaporation. It should be pointed out that in application of the *Mahrt and Pan* [1984] scheme, the conclusions of *Mahrt and Pan* [1984] hold good for clay type of soils and will not work for sand. The soil type in our application is silt loam whose properties are closer to clay than to sand, hence the appropriateness of this approach.

The hydrological model is applied over a 10 year period. The observed daily streamflows from 1980 to 1984 are used to calibrate the model parameters. The simulated streamflows are validated over the 1985–1989 period. The comparisons between observed and simulated streamflows have been good given the fact that the rain gage used for rainfall input was about 16 km away from the catchment. The aim of this paper was not to develop a model for accurate streamflow prediction. The aim of this paper is to develop a scheme to predict the surface temperature and soil moisture with a sufficient degree of accuracy for the 1 cm surface layer. The streamflow is compared to determine that the hydrological model behaves properly with the rainfall process. The model-simulated soil moistures and surface temperatures are compared for the time periods during the four IFCs in FIFE. This model produces values of the 1 cm layer soil moistures which agree with our understanding of hydrology. This hydrological model shows a definite promise in estimating soil moisture and can be used along with microwave satellite data.

The 19 and 37 GHz polarization difference indices have a greater range between the residual and the saturated soil moisture levels, showing greater sensitivity to soil moisture variations. The sensitivity of the polarization difference index to the soil moisture is affected by the leaf area index; an increase in leaf area index decreases this sensitivity; an increase in soil moisture results in increased sensitivity followed by a decrease in sensitivity at high soil moistures. Among the vegetation parameters, the stem area index and the canopy moisture content affect the polarization difference the greatest. An increase in the stem area index and/or the canopy moisture content results in a masking of the polarization difference signal originating at the soil surface. We wish to caution the reader(s) that a straight forward regression type of analysis (between soil moisture and polarization difference index) may not work without due attention to the sensitivities and uncertainties that are studied in this paper. Ignoring these may result in incorrect results.

It is proposed that this model can be used in conjunction with passive microwave satellite data for soil moisture estimation. The 19 and 37 GHz Special Sensor Microwave Imager (SSM/I) brightness temperature data are proposed to be used for the study. This does not imply that the microwave brightness temperature data are the only way to estimate soil moistures. We would emphasize at this point that the use of satellite data is useful given its spatial and temporal coverage, and it can be used in conjunction with hydrological modeling to achieve better estimates of soil moisture. Microwave satellite data at lower frequency (6.6 GHz) has been used in the past to infer soil moisture [*Owe et al.*, 1992] and soil wetness [*Choudhury and Monteith*, 1988]. These, however, use simple regression-based relations between soil moisture (or antecedent precipitation index API) and brightness temperature. In the case of higher frequencies (such as the 19 and 37 GHz frequencies that we propose to use), a simple inversion may not be very effective. It is desired that a complete model of soil hydrology providing the surface temperature and soil moisture along with a radiative transfer model for the plant canopy and an attenuation model for the atmosphere would be used to simulate the SSM/I brightness temperature and subsequently help in retrieving soil moistures from observed brightness temperatures. The model of thin layer soil hydrology will help in this regard.

Acknowledgments. The page charges were paid by the Sounder Research Team (Joel Susskind). This is gratefully acknowledged.

References

Baret, F., and G. Guyot, Potentials and limits of vegetation indices for LAI and APAR assessment, *Remote Sens. Environ.*, *35*, 161–173, 1991.

Bras, R. L., *Hydrology: An Introduction to Hydrologic Science*, Addison-Wesley, Reading, Mass., 1990.

Brooks, R. H., and A. T. Corey, Hydraulic properties of porous media, *Hydrol Pap. 3*, Colo. State Univ., Fort Collins, Colo., 1964.

Brutsaert, W., *Evaporation Into the Atmosphere. Theory, History and Applications*, D. Reidel, Norwell, Mass., 1982

Chandrashekar, S., *Radiative Transfer*, Dover, Mineola, New York, 1960

Choudhury, B. J., Reflectivities of selected land surface types at 19 and 37 GHz from SSM/I observations, *Remote Sens Environ.*, *46*, 1–17, 1993.

Choudhury, B. J., and J. L. Monteith, A four-layer model for the heat budget of homogeneous land surfaces, *Q. J. R. Meteorol. Soc.*, *114*, 373–398, 1988.

Choudhury, B. J., J. R. Wang, A. Y. Hsu, and Y. L. Chien, Simulated and observed 37 GHz over Africa, *Int. J. Remote Sens.*, *11*(10), 1837–1868, 1990.

Dickinson, R. E., Modeling evapotranspiration for three-dimensional global climate models, in *Climate Processes and Climate Sensitivity*, *Geophys. Monogr. Ser.*, vol. 29, edited by J. E. Hansen and T. Takahashi, pp. 58–72, AGU, Washington, D. C., 1984.

Dubayah, R., Estimating net solar radiation using Landsat Thematic Mapper and digital elevation data, *Water Resour. Res.*, *28*, 2469–2484, 1992.

Dubayah, R., J. Dozier, and F. W. Davis, Topographic distribution of clear-sky radiation over the Konza Prairie, Kansas, *Water Resour. Res.*, *26*, 679–690, 1990.

Eagleson, P. S., *Dynamic Hydrology*, McGraw Hill, New York, 1970.

Eagleson, P. S., Ecological optimality in water limited natural soil-vegetation systems, 1, Theory and hypothesis, *Water Resour. Res.*, *18*(2), 325–340, 1982.

Famiglietti, J. S., and E. F. Wood, Multiscale modeling of spatially variable water and energy balance processes, *Water Resour. Res.*, *30*(11), 3061–3078, 1994a.

Famiglietti, J. S., and E. F. Wood, Application of multiscale water and energy balance models on a tall grass prairie, *Water Resour. Res.*, *30*, 3079–3093, 1994b

Francini, M., and M. Pacciani, Comparative analysis of several conceptual rainfall-runoff models, *J. Hydrol.*, *122*, 161–219, 1991

Goward, S. N., S. Turner, D. G. Dye, and S. Liang, The University of Maryland improved global vegetation index product, *Int. J. Remote Sens.*, *15*(17), 3365–3395, 1994.

Hollinger, J. P., J. L. Peirce, and G. A. Poe, SSM/I instrument evaluation, *IEEE Trans. Geosci. Remote Sens.*, *28*(5), 781–790, 1990.

Idso, S. B., A set of equations for full spectrum and 8–14 μm and 10.5–12.5 μm thermal radiation from cloudless skies, *Water Resour. Res.*, *17*, 295–304, 1981.

Lakshmi, V., Use of special sensor microwave imager data for soil

moisture estimation, Ph.D. thesis, Princeton Univ., Princeton, New Jersey, 1995.

Lakshmi, V., E. F. Wood, and B. J. Choudhury, Investigation of effect of heterogeneities in vegetation and rainfall on simulated SSM/I brightness temperatures, to *Int. J. Remote Sens.*, in press, 1996a.

Lakshmi, V., E. F. Wood, and B. J. Choudhury, Evaluation of SSM/I data for regional soil moisture estimation over the Red River basin, *J. Clim.*, in press 1996b.

Lanicci, J. M., T. N. Carlson, and T. T. Warner, Sensitivity of the Great Plains severe storm environment to soil moisture distribution, *Monthly Weather Review*, 115, pp 2660–2673, 1987.

Larcher, W., *Physiological Plant Ecology*, Springer-Verlag, New York, 1975.

Liang, X., D. P. Lettenmaier, E. F. Wood, and S. J. Burges, A simple hydrologically based model of land surface water and energy fluxes for general circulation models, *J. Geophys. Res.*, *99*, 14,415–14,428, 1994.

Mahfouf, J. F., E. Richard, and P. Mascart, The influence of soil and vegetation on mesoscale circulations, *J. Clim. Appl. Meteorol.*, *26*, 1483–1495, 1987.

Mahrt, L., and H. Pan, A two-layer model of soil hydrology, *Boundary Layer Meteorol.*, *29*, 1–20, 1984.

Neghassi, H. M., Crop water use in yield models with limited soil moisture, Ph.D. dissertation, Colo. State Univ., Fort Collins, Colo., 1974.

Owe, M., A. A. van De Griend, and A. T. C. Chang, Surface soil moisture and satellite microwave observations in semi-arid southern Africa, *Water Resour. Res.*, *28*(3), 829–839, 1992.

Rawls, W. J., D. L. Brakensiek, and K. E. Saxton, Estimation of Soil Water Properties, *Trans. Am. Soc. Agric. Eng.*, *25*, 1316–1320, 1982.

Rutter, A. J., A. J. Morton, and P. C. Robins, A predictive model of rainfall interception in forests, II, Generalization of the model and comparison with observations in some coniferous and hardwood stands, *J. Appl. Ecol.*, *12*, 367–380, 1975.

Schmugge, T., Remote sensing of soil moisture, in *Hydrological Forecasting*, edited by M. G. Anderson and T. P. Burt, John Wiley, New York, 1985.

Sellers, P. J., Y. Mintz, Y. C. Sud, and A. Dalcher, A simple biosphere model for use within general circulation models, *J. Atmos. Sci.*, *43*, 505–531, 1986.

Sellers, P. J., F. G. Hall, G. Asrar, D. E. Strebel, and R. E. Murphy, An overview of the First International Satellite Land Surface Climatology Project (ISLSCP) Field Experiment (FIFE), *J. Geophys. Res.*, *97*, 18,345–18,371, 1992.

Stephens, G. L., Radiative transfer through arbitrarily shaped optical media, I, A general method of solution, *J. Atmos. Sci.*, *45*, 1818–1836, 1988.

Tennessee Valley Authority (TVA), Heat and mass transfer between a water surface and the atmosphere, *Lab. Rep. 14*, 1972.

Ulaby, F. T., R. K. Moore, and A. K. Fung, *Microwave Remote Sensing*, vol. 1, Addison-Wesley, Reading, Mass., 1981.

Ulaby, F. T., R. K. Moore, and A. K. Fung, *Microwave Remote Sensing: Active and Passive, From Theory to Applications*, vol. 3, Artech House, Dedham, Mass., 1986.

Wang, J. R., and T. J. Schmugge, An empirical model for the complex dielectric permissivity of soils as a function of water content, *IEEE Trans. Geosci. Remote Sens.*, *18*(4), 288–295, 1980.

Whittaker, R. W., and G. M. Woodwell, Surface area relations of woody plants and forest communities, *Am. J. Bot.*, *54*, 931–939, 1967.

Whittaker, R. W., F. H. Bormann, G. E. Likens, and T. G. Siccama, The Hubbard Brook ecosystem study: Forest biomass and production, *Ecol. Monogr.*, *44*, 232–252, 1974.

Wood, E. F., Advances in land surface modeling, *U.S. Natl. Rep. Int. Union Geod. Geophys., 1987–1990, Rev. Geophys.*, *29*, 193–201, 1991.

Zhang, D. L., and R. A. Anthes, A high resolution model of the planetary boundary layer—Sensitivity tests and comparisons with SESAME-79 data, *J. Appl. Meteorol.*, *21*, 1594–1609, 1982.

B. J. Choudhury, Hydrological Sciences Branch, Code 974, NASA Goddard Space Flight Center, Greenbelt, MD 20771.

V. Lakshmi, General Sciences Corporation, Laboratory for Atmospheres, Code 910.4, NASA Goddard Space Flight Center, Greenbelt, MD 20771.

E. F. Wood, Water Resources Program, Department of Civil Engineering and Operations Research, Princeton University, Princeton, NJ 08544.

(Received August 12, 1996; revised November 14, 1996;
accepted December 2, 1996.)